Conformational changes of the multifunction p97 AAA ATPase during its ATPase cycle

Isabelle Rouiller[1,2], Byron DeLaBarre[3], Andrew P. May[4,5], William I. Weis[4], Axel T. Brunger[3], Ronald A. Milligan[1] and Elizabeth M. Wilson-Kubalek[1]

Published online 18 November 2002; doi:10.1038/nsb872

p97 (also called VCP), a member of the AAA ATPase family, is involved in several cellular processes, including membrane fusion and extraction of proteins from the endoplasmic reticulum for cytoplasmic degradation. We have studied the conformational changes that p97 undergoes during the ATPase cycle by cryo-EM and single-particle analysis. Three-dimensional maps show that the two AAA domains, D1 and D2, as well as the N-domains, experience conformational changes during ATP binding, ATP hydrolysis, P_i release and ADP release. The N-domain is flexible in most nucleotide states except after ATP hydrolysis. The rings formed by D1 and D2 rotate with respect to each other, and the size of their axial openings fluctuates. Taken together, our results depict the movements that this and possibly other AAA ATPases can undergo during an ATPase cycle.

The ubiquitous ATPase p97 (also called vasolin-containing protein (VCP) in animals; VAT in *Archaebacteria* and cdc48 in yeast) is abundant in all cells (comprising ~1% of the cell cytosol)[1] and participates in several essential cellular functions. p97 has been implicated in post-mitotic homotypic membrane fusion of the endoplasmic reticulum and the Golgi apparatus[2,3], assembly and growth of the nucleus[4], apoptosis[5,6] and DNA replication[7,8]. It is also involved in the ubiquitin/proteasome-dependent degradation pathway[9–12], as well as the extraction of misfolded lumenal and membrane proteins from the endoplasmic reticulum for cytosolic degradation[13–16].

Several lines of evidence suggest that binding of alternative cofactors determines the specific role of p97. Thus far, several cofactors have been identified: p47 (a 47 kDa protein essential in p97-mediated membrane fusion)[17,18], DUF (DNA unwinding factor)[8]; Ufd1 (ref. 10), Ufd2 (ref. 19) and Ufd3 (proteins involved in the ubiquitin fusion degradation pathway or ufd)[20]; and SVIP (small VCP interacting protein; reviewed in ref. 21). Ufd1 interacts with p97 in a complex with Npl4 (a protein involved in nuclear protein localization)[10]. Moreover, p47 and Npl4–Ufd1 bind to p97 in a mutually exclusive manner[10].

p97 is a member of the AAA family (ATPases associated with different cellular activities[22]). AAA proteins contain either one (type I), such as katanin, RuvB and HslU, or two (type II), such as p97 and NSF, AAA domains per subunit. The AAA domains have a conserved structural fold consisting of a nucleotide-binding N-terminal subdomain and a helical C-terminal subdomain[23,24]. These proteins typically assemble into oligomers and seem to have the conserved function of converting the energy from ATP hydrolysis into mechanical force. Several mechanisms have been proposed for how the chemically stored energy is transformed into action[21,25].

Each p97 protomer contains an N-terminal domain followed by two AAA domains, D1 and D2. The N-domains of p97, VAT and NSF show a similar fold despite low sequence identity[26–29]. Because the N-domain is thought to be the principal means of interaction with target molecules, the fold similarity suggests a conserved mechanism of interaction. There is no atomic structure for the full-length p97 complex so far. However, a hexamer of N–D1 domains with ADP bound has been solved by X-ray crystallography[30]. No tertiary structural information exists for the D2 domain, but with ~40% sequence identity to D1, it probably possesses a similar fold. The quaternary structures of p97 and VAT investigated by electron microscopy (EM) show that the proteins form a barrel-like structure with the two AAA domains arranged on top of each other, each forming a hexameric ring[30–33]. The substrate-binding N-domains of p97 have been difficult to observe by EM, suggesting that they are flexible[30–33]. However, the N-domains were visualized in a recent study of VAT in the absence of nucleotide[34].

By comparing projection maps from cryo-EM images of p97 in different nucleotide conditions, we have demonstrated that p97 undergoes a large conformational change upon nucleotide binding[33]. Zhang and colleagues[30] proposed a conformational change between the ATP- and ADP-bound states of p97 by comparing their atomic structure of the D1 domain of p97 with the atomic structure of the D2 domain of the homologous protein NSF[35,36].

To further investigate the conformational changes of the p97 during the ATPase cycle, we have studied the full-length protein and an N-terminally truncated mutant containing only the two AAA domains (ΔN-p97). We have calculated three-dimensional (3D) maps of the full-length and the truncated mutant in the presence of various nucleotides using cryo-EM and single-particle image analysis.

Hexameric state

The full-length p97 and the ΔN-p97 mutant (Fig. 1*a*) were studied by cryo-EM in the absence of nucleotide (apo) and in the

[1]The Department of Cell Biology, The Scripps Research Institute, 10550 North Torrey Pines Road, La Jolla, California 92037, USA. [2]Current address: The Burnham Institute, 10901 North Torrey Pines Road, La Jolla, California 92037, USA. [3]Howard Hughes Medical Institute and Departments of Molecular and Cellular Physiology, Neurology and Neurological Sciences, and Stanford Synchrotron Radiation Laboratory, Stanford University, Stanford, California 94305-5489, USA. [4]Departments of Structural Biology and Molecular and Cellular Physiology, Stanford University, Stanford, California 94305-5126, USA. [5]Current address: Signature Bioscience, 475 Brannan Street, San Francisco, California 94107, USA.

Correspondence should be addressed to E.M.W.-K. *email: kubalek@scripps.edu*

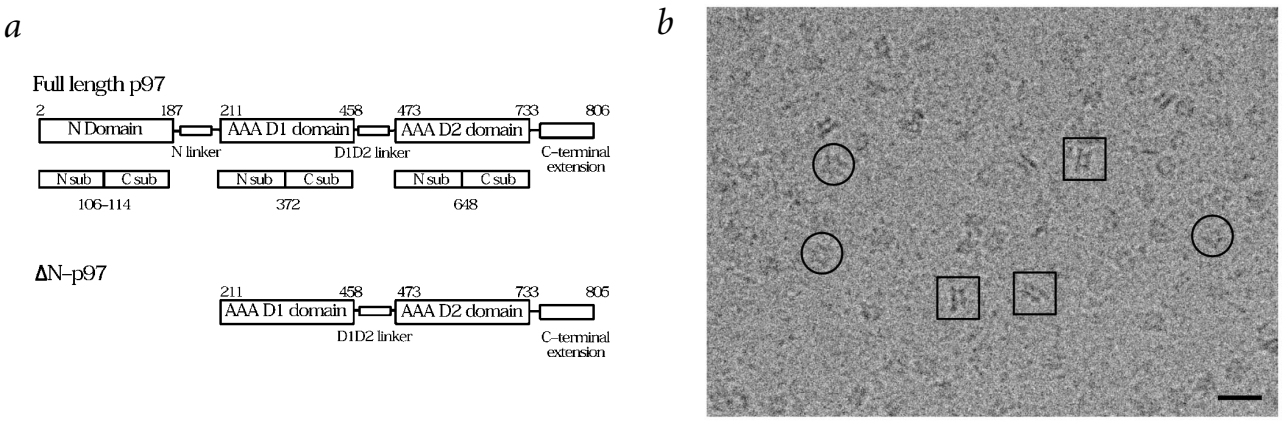

Fig. 1 p97 and ΔN-p97. ***a***, Schematic representation of the different domains and subdomains of the full-length p97 monomer and the N-terminally truncated mutant, ΔN-p97. ***b***, Cryo-EM showing a field of p97 incubated with ADP-AlF_x and examples of side views (boxed) and en-face orientation (circled). Scale bar = 200 Å.

presence of AMP-PNP (a non-hydrolyzable ATP analog), ADP-AlF_x (a transition state analog for the hydrolysis step)[37] and ADP. Both p97 and ΔN-p97 formed hexameric complexes in all of the above nucleotide conditions. Gel filtration and light-scattering experiments confirmed the hexameric state of p97 and ΔN-p97 (data not shown).

Both p97 and ΔN-p97 complexes adopted several orientations on the cryo-EM grids. Characteristic side views of the particles[31] were frequently observed (Fig. 1*b*). Images were analyzed by standard single particle procedures (see Methods) to generate 3D maps of p97 and ΔN-p97 in various nucleotide conditions. Previously, we have demonstrated the six-fold symmetry of p97 in all nucleotide conditions by rotational power spectrum analysis[33]. We have extended this result to the present 3D analysis and have applied the six-fold symmetry to calculate the 3D maps.

General structure of p97 and ΔN-p97

The surface rendering of the 3D maps of p97 (Fig. 2) and ΔN-p97 (Fig. 4*a*) shows that both complexes are composed of two stacked hexameric rings forming a barrel-like structure with ~120–160 Å diameter and ~80–90 Å high. The bottom rings (~130–145 Å diameter) are slightly larger than the top rings (~120–135 Å diameter) and, with the exception of p97–ADP-AlF_x, the apparent size of their axial openings are also larger (~45–65 Å diameter) than those of the top rings (~25 Å diameter). Six additional side protrusions extending out to a radius of ~80 Å are associated with the bottom ring near the central plane of the structure. The p97–ADP-AlF_x structure is unique in that in addition to the common structural elements, additional densities (accounting for about one-third of the total protein mass) were observed surrounding the top ring (Fig. 2*c*). No such densities were observed in any of the nucleotide conditions for ΔN-p97 (Fig. 4*a*). This strongly suggests that the extra mass corresponds to the N-domains.

The thresholds used to render the ΔN-p97 and p97–ADP-AlF_x volumes were chosen such that the surface enclosed the expected molecular mass of the constructs (412 kDa and 558 kDa, respectively) and corresponds to a contouring level in which no unconnected densities were observed. When a threshold corresponding to 558 kDa was used for the p97-apo, p97–AMP-PNP and p97–ADP volumes, unconnected densities located above the hexameric rings were observed. The shape and strength of these unconnected densities varied among independent 3D maps calculated in the same nucleotide conditions. These densities disappeared when the threshold corresponding to 412 kDa was used. Therefore, this threshold was used to render the volumes of p97-apo, p97–AMP-PNP and p97–ADP.

Conformational changes of p97

To investigate the possible conformational changes that may occur during the ATPase cycle, we studied p97 in defined nucleotide states using saturating amounts of nucleotides or nucleotide analogs (~1,000-fold over the number of nucleotide-binding sites). Although the conformational changes observed may not correlate with the true functional states of the reaction cycle *in vivo*, the conformational changes observed provide insights into the possible movements and their driving force. To compare the conformational changes, we aligned the maps so that features in the top rings were co-incident. This allowed the size variation of the axial openings and rotation of the different domains with respect to each other to be seen clearly (Fig. 3; movie at *http://www.scripps.edu/milligan/kubalek/p97.html*).

ATP binding. To understand the conformational changes during ATP binding, we compared the structure of p97-apo with that of p97–AMP-PNP. Remarkably, the N-domains are flexible and not clearly visualized in both nucleotide states. Binding of AMP-PNP leads to subunit rearrangements in both the top and bottom rings of p97, resulting in more compact rings that maintain the size of their axial openings. The diameters of the two rings of the p97–AMP-PNP volume are smaller by ~10 Å than those of p97-apo (Fig. 3a). The top rings of both structures are almost identical at the observed resolution (Fig. 3*a* row ii). The conformational change is more pronounced in the bottom ring, which is more compact and less scalloped (Figs 2*b*, 3*a* row iv). Additionally, upon binding of AMP-PNP, the side protrusions rotate around the six-fold axis clockwise by ~3° (curved arrow, Fig. 3*a* row iii) and the bottom ring rotates clockwise by ~8° (curved arrow, Fig. 3*a* row iv). Projection maps calculated from the 3D maps of p97-apo and p97–AMP-PNP were identical to the projection maps previously calculated from top views of p97, indicating that the observed changes in the 3D structure explain the major conformational change of the full-length p97 upon nucleotide binding observed in our 2D study[33].

Nucleotide hydrolysis. The conformational changes of p97 during nucleotide hydrolysis were studied by comparing the structures of p97–AMP-PNP and p97–ADP-AlF_x. The most obvious

change during nucleotide hydrolysis is that the N-domains of p97–ADP–AlF_X in both complexes become ordered and are clearly visible (extra densities around the top ring of p97–ADP-AlF_x, N; Figs 2*c*, 3*b*). In addition to this major change, other differences are apparent. In particular, the height of p97–ADP-AlF_x is slightly smaller than that of p97–AMP-PNP and the side protrusions have tilted down towards the bottom of the structure (arrow down, Fig. 3*b* row *i*). The side protrusions have also rotated by ~3° clockwise (Fig. 3*b* row *iii*) and the bottom ring counter clockwise by ~8° (Fig. 3*b* row *iv*). The axial opening of the bottom ring becomes as small as the axial opening of the top ring, resulting in a slight closure of the central cavity near the bottom of the structure.

Phosphate release. Comparing the p97–ADP-AlF_x and p97–ADP maps reveals changes that occur upon phosphate release (Fig. 3*c*). The most dramatic change at this step in the ATPase cycle is that the densities corresponding to the N-domains are once again weak and unconnected to the barrel, suggesting that the N-domains have become mobile. The axial opening of the top ring appears to have closed (Fig. 3*c* row *ii*). The axial opening of the bottom ring has reopened, compared with p97–ADP-AlF_x, and is similar in size to that of p97–AMP-PNP (Fig. 3*c* row *iv*). The side protrusions have tilted back to their initial position (arrow up, Fig. 3*c* row *i*) and have also rotated counterclockwise by ~6° (curved arrow, Fig. 3*c* row *iii*). The bottom ring has rotated clockwise by ~10° (curved arrow, Fig. 3*c* row *iv*).

ADP release. Finally, to complete the cycle and reveal the conformational changes upon ADP release, we compared the structures of p97–ADP with p97-apo (Fig. 3*d*). At this ADP release step, the top ring becomes slightly larger and its axial opening reclaims its original size (Fig. 3*d* row *ii*), the side protrusions do not move and the bottom ring rotates counterclockwise by ~10°.

Overall, our data suggest that during the ATPase cycle, the bottom ring rotates around the six-fold axis back and forth with respect to the top ring by a maximum of 10°, and the side protrusions rotate back and forth by a maximum of 6°. The N-domains are flexible in all conditions except in the presence of ADP-AlF_x, where they become clearly visible. Furthermore, the small axial opening at the top of the central cavity is of constant diameter during ATP binding and hydrolysis but appears to close completely upon P_i release. The larger axial opening of the bottom rings also remains constant except after ATP hydrolysis, when it appears as closed as that of the top ring. This fluctuation of the size of the axial openings in the top and bottom rings also translates into size variation of the central cavity.

Conformational changes of ΔN-p97

The conformational changes observed in the top and bottom domains of p97 throughout the ATPase cycle were not observed in ΔN-p97. The surface rendering of the ΔN-p97-apo, ΔN-p97–AMP-PNP, ΔN-p97–ADP-AlF_x and ΔN-p97–ADP maps were identical with a threshold corresponding of 412 kDa. A higher threshold revealed slight movements of the centers of mass. The significance of these movements is unclear at the present resolution. This result was unexpected because the ΔN-p97 mutant has an ATPase activity comparable to that of the full-length protein (S.W. Whiteheart, pers. comm.) and, therefore, can presumably exist in the different nucleotide states. This result implies that, although the N-domains are not necessary for ATPase activity, they operate together with the top and bottom domains to generate nucleotide-induced conformational changes.

Discussion

In the present study, we have calculated 3D maps of p97 and ΔN-p97 in different nucleotide conditions mimicking the four major steps of the ATPase cycle. Unlike other AAA ATPases, such as katanin and NSF[25], p97 assembles into a hexamer in all nucleotide conditions. Likewise, ΔN-p97 forms hexamers in all nucleotide conditions, demonstrating that the N-domains are not required for hexamerization, similar to the behavior of VAT[32]. So far, only two atomic structures of type I AAA ATPases have been solved in different nucleotide states: RuvB has been solved in both the ADP and ATP states[38] and HslU has been studied in several nucleotide conditions, although some controversy exists about the exact identity of the bound nucleotide in these structures[39–42]. Detailed kinetics of ligand binding to the 12 nucleotide binding sites in p97 are not known, and relative occu-

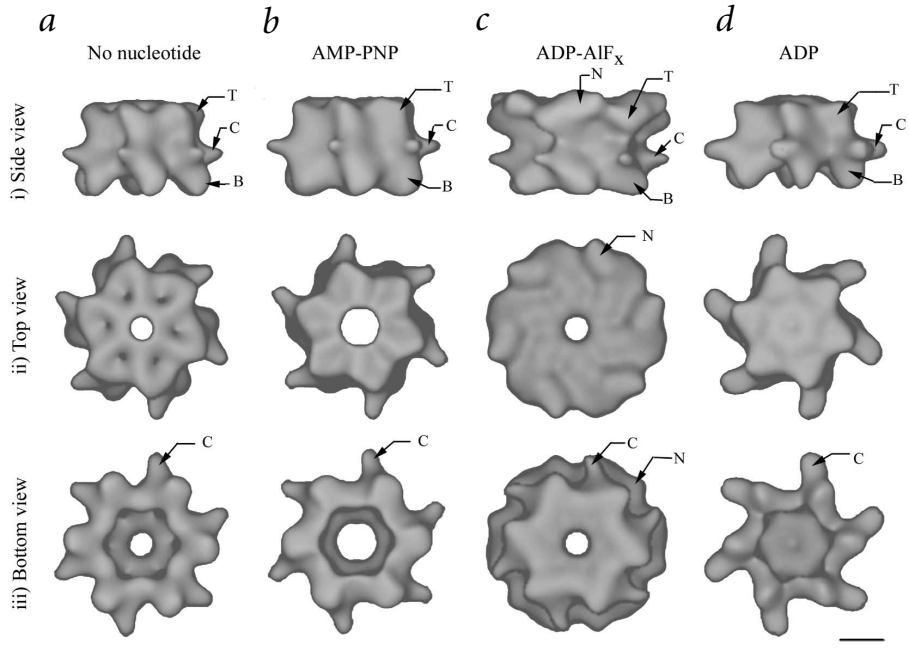

Fig. 2 Structure of p97 in different nucleotide conditions. Isosurface representations of the 3D EM maps of ***a***, p97-apo; ***b***, p97–AMP-PNP; ***c***, p97–ADP-AlF_x; and ***d***, p97–ADP obtained by cryo-EM and single particle processing, after low-pass filtering to 24 Å. Rows *i*, *ii* and *iii* show the 3D maps in the side, top and bottom view orientations, respectively. These orientations emphasize the main features: top ring (T), side protrusions (C), bottom ring (B) and the additional densities (N) seen in p97–ADP-AlF_x (c). Varying the threshold used to contour the p97–AMP-PNP, p97–ADP and p97-apo (at least from that corresponding to molecular weight of ~350–600 kDa) always resulted in the diameter of the hole in the bottom ring (B) being larger than that of the top ring (T). Identical variation of the threshold used to contour the p97–ADP-AlF_x always resulted in the holes of top and bottom rings being of equal size. This indicates that the differences in the size of the holes observed is not an artifact of the threshold used. Scale bar = 40 Å.

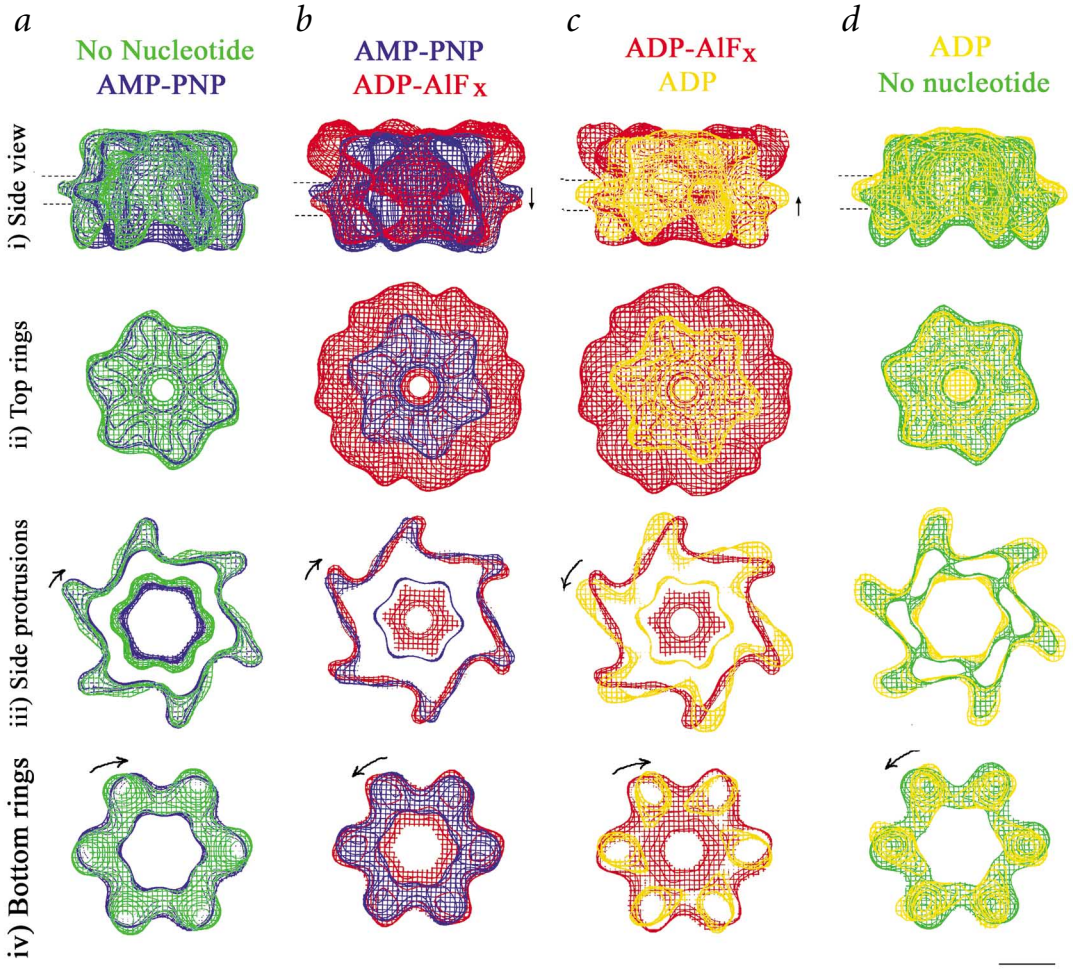

Fig. 3 Conformational changes of p97. Comparison of the isosurface representations of p97-apo (green), p97–AMP-PNP (blue), p97–ADP-AlF$_x$ (red) and p97–ADP (yellow) representing the conformational changes that the molecule undergoes upon ***a***, ATP binding; ***b***, nucleotide hydrolysis; ***c***, phosphate release; and ***d***, ADP release. The top rings of the different volumes were aligned and two volumes, as viewed in O[48], are shown facing up and superimposed in each image. The superimposed volumes are shown in a side view orientation (row *i*). Representative sections of the volumes, taken perpendicular to the six-fold axis, were selected such as to show independently the top rings (row *ii*), the side protrusions (row *iii*) and the bottom rings (row *iv*). The planes of sectioning are indicated as dotted lines in the side view representations (row *i*). Domain movement and relative rotation of the side protrusions and the bottom rings are indicated (arrows). Scale bar = 40 Å.

pancy may play a functional role *in vivo*, as was suggested for the HslU AAA ATPase[42]. Indeed, there is no reason to believe that all the 12 AAA domains contain the same nucleotide *in vivo*, and there may be allosteric regulation between the 12 nucleotide-binding sites. However, we have taken the simple approach of examining p97 in the presence of a large excess of defined nucleotides or nucleotide analogs. Such studies are important because they provide a first glimpse of the possible nucleotide-mediated conformational changes.

Movement of the N-domains

Densities corresponding to the N-domains of p97 were observed only in the presence of ADP-AlF$_x$, suggesting that they have a fixed location and conformation with respect to the top and bottom rings in this state. In the other nucleotide conditions, no densities could be confidently attributed to the N-domains. Flexibility of the N-domains has been observed by EM in p97–ADP[30] and may be allowed by the linker between the N and D1 domains. This observation is also reminiscent of the p97–p47 complex, where the N-domains of p97 become locked into a rigid position only in the presence of AMP-PNP or ATP[33]. In contrast to these solution results, the crystal structure of the N-D1 hexamer in the presence of ADP[30] (p97-ND1–ADP) showed ordered N-domains that obey hexameric symmetry. This difference may be a consequence of crystal lattice packing restrictions or perhaps is due to the absence of the D2 domain in the crystal structure.

We attempted to fit the atomic structure of the p97-ND1–ADP hexamer[30] into EM densities of p97–ADP-AlF$_x$ (data not shown). When the D1 domains were fit into the central EM densities, the surrounding N-domains did not fit well into the peripheral EM densities. This indicates that the molecular arrangement of the N-domains in p97–ADP-AlF$_x$ differs from the crystal packing arrangement of p97-ND1–ADP[30]. The simplest explanation for this is the difference in nucleotide, although an influence by D2 is also possible.

Movement of the top and bottom rings

We have shown that the top and bottom rings rotate with respect to each other during the ATPase cycle (Fig. 3). We have also

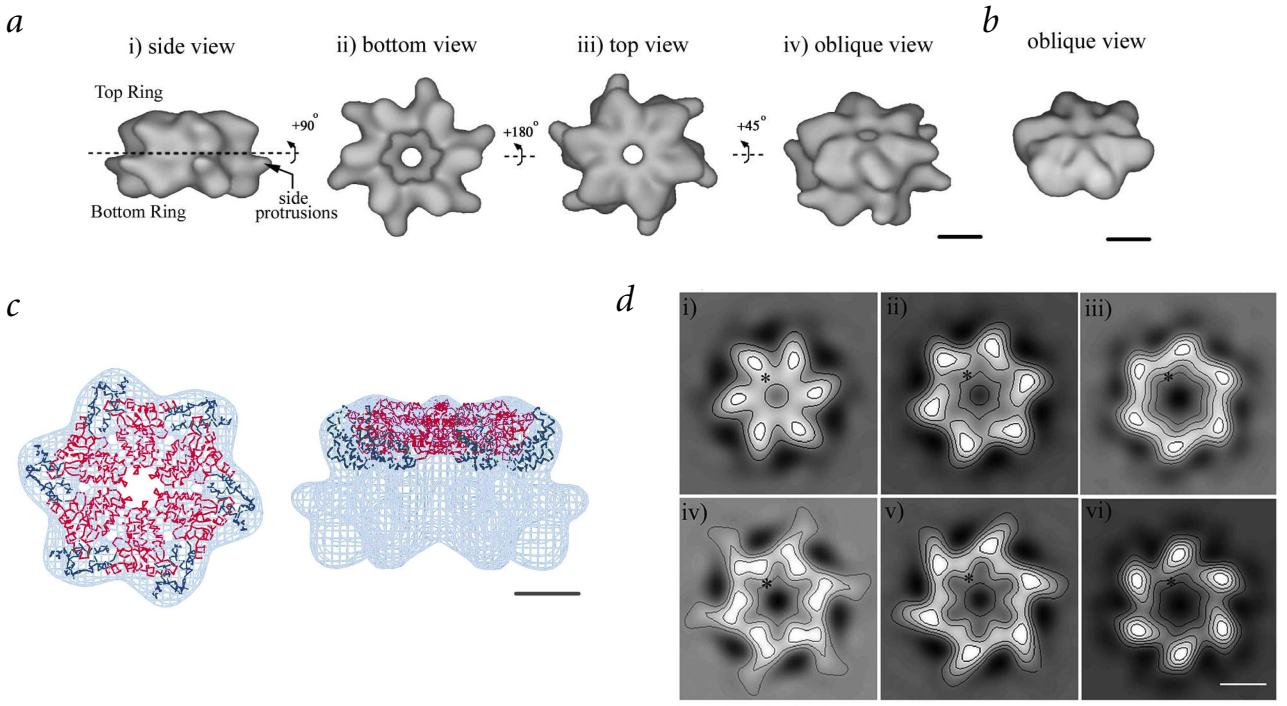

Fig. 4 Stucture of ΔN-p97. ***a***, Isosurface representations of ΔN-p97–AMP-PNP map obtained by cryo-EM and single particle analysis, after low-pass filtering to 24 Å. ***b***, Isosurface representation of the D1 domain of p97 as it appears in the p97-ND1–ADP X-ray structure. The D1 domains from the PDB file (PDB entry 1E32)[30] were imported to SPIDER[45], converted into density and low-pass filtered at 24 Å resolution. ***c***, Fitting of the D1 atomic structure[30] into the EM map density (cyan). The four-helix bundle C subdomains (dark blue) are located at the corner of the hexameric ring while the wedge shaped N subdomains (red) are located more centrally. ***d***, Sections (4.1 Å thick) of the ΔN-p97–AMP-PNP map taken perpendicular to the axis of symmetry shown in a gray scale representation with superposed contour plots, selected from the top (*i*), middle (*ii*) and bottom (*iii*) of the top ring, and from the top (*iv*), middle (*v*) and bottom (*vi*) of the bottom ring. The protein densities are shown as white with a dark background. Densities near the centers (asterisk) are similar in shape but are more diffuse in the bottom ring compared the equivalent densities in the top ring. Scale bar = 40 Å.

shown that both rings of the p97 complex become slightly smaller and more compact upon addition of AMP-PNP, suggesting a packing rearrangement within each D1 and D2 hexamer. Because the C subdomains of the AAA modules are located at the periphery of the hexamers (Fig. 4*c*), the reduction in size of the D1 and D2 hexamers could be due to the movement of the C subdomain with respect to the N subdomain of the AAA module, in a manner similar to that described for HslU[42] and RuvB[38].

We have also shown that the sizes of the axial opening of the top and bottom rings vary during the ATPase cycle (Fig. 3). The apparent size variation could be due to the mobility and/or rearrangement of the structural domains located near the centers, namely the N subdomains of the D1 and D2 AAA domains. In VAT[34], the N-domains are visible, and the sizes of the axial openings of the top and bottom rings of VAT are identical in the absence of nucleotide. This conformation is most similar to p97–ADP-AlF$_x$, suggesting that these two proteins behave differently upon addition of nucleotide.

In vivo genetic studies have shown that both AAA domains of the trypanosome p97 do not need to be active[43]. Mutations impairing the D1 ATPase activity were still viable, whereas mutations impairing D2 ATPase activity were lethal. This suggests that conformational changes can be transmitted through the impaired D1 to the distant N-domains, implying long-range allostery.

Assigning N, D1 and D2 to the EM maps

The additional densities surrounding the top ring of p97–ADP-AlF$_x$ were not observed in any ΔN-p97 maps, indicating that they correspond to the ~30 kDa N-domains of p97. The absence of the well-defined densities surrounding the top ring of p97-apo, p97–AMP-PNP and p97–ADP suggests that the N-domains are mobile at these steps in the ATPase cycle.

Identification of the top and bottom rings as the D1 and D2 domains, respectively, is based on two lines of evidence. First, the X-ray structure of N–D1 shows that the N-domains have extensive interactions at the periphery of the D1 hexamer, similar to the situation visualized in our p97–ADP-AlF$_x$ map. Second, the atomic structure of the D1 hexamer fits snugly within the top ring (Fig. 4*c*) and not so well within the bottom ring and, when smoothed to 24 Å resolution, shows the same surface features as the top ring (Figs 2 row *ii*, 4*a* panel *iv* and 4*b*).

The differences observed between the D1 and D2 rings of ΔN-p97 and full-length p97 volumes were surprising given the high sequence identity (~40%) between these two domains. To further illustrate the similarities and differences of the top and bottom rings, sections of the ΔN-p97 map were taken perpendicular to the six-fold symmetry axis through the top, middle and bottom of each ring (Fig. 4*d*). The side view of the volume (Figs 2 row *i*, 4*a* panel *i*) and the sections (Fig. 4*d*) show densities with similar shape and orientation, indicating that the top and bottom rings have the same handedness, suggesting a head-to-tail arrangement of D1 and D2 domains. The top view of the volume (Fig. 2 row *ii*) and the depicted sections show that the two rings are not in register one on top of the other, but that the bottom ring is rotated counterclockwise around the axis of symmetry with respect to the top ring (viewed from the top of the structure). The densities near the center of the bottom ring are more diffuse than the equivalent densities in the top ring (aster-

Table 1 Summary of the data acquired and used for the reconstructions

3D EM map	Data acquired on film or CCD	Total number of particles selected	Total number of particles used in final refinement[1]	Defocus (μm) and number of particles included in final refinement (in brackets)	Final resolution after CTF correction (Å)[2]
ΔN-p97– AMP-PNP	Film[3]	11,340	3,003	1.5 (995), 1.6 (1,060), 1.7 (948)	24
ΔN-p97–AMP-PNP	CCD[3]	6,378	2,188	1.2 (250), 1.3 (1,418), 1.4 (400), 1.5 (120)	25
ΔN-p97–ADP-AlF_x	Film	5,525	2,523	1.4 (524), 1.7 (1,418), 1.8 (581)	24
ΔN-p97–ADP	Film	9,160	2,978	1.65 (2,978)	19
ΔN-p97-apo	Film	4,570	2,702	1.75 (2,702)	19
p97–AMP-PNP	CCD	11,690	3,008	1.1 (135), 1.2 (216), 1.3 (519), 1.4 (805), 1.5 (852), 1.6 (230), 1.7 (136), 1.8 (81), 1.9 (34)	24
p97–ADP-AlF_x	CCD	12,586	3,134	1.2 (181), 1.3 (429), 1.4 (957), 1.5 (1,052), 1.6 (391), 1.7 (91), 1.8 (33)	24
p97–ADP	CCD	6,537	2,763	1.1 (38), 1.2 (66), 1.3 (679), 1.4 (553), 1.5 (424), 1.6 (371), 1.7 (338), 1.8 (93), 1.9 (201)	24
p97-apo	CCD	8,189	2,760	1.1 (333), 1.2 (1,340), 1.3 (908), 1.4 (100), 1.8 (79)	22

[1]The 3D maps calculated including all the particles selected were identical to the maps calculated reducing the number of particles per view.
[2]The resolution of the final map, estimated by the Fourier shell correlation of 0.5, is indicated. A comparison with the X-ray structure of D1 (ref. 30), low-pass filtered at various resolutions, confirmed that all the maps were ~24 Å resolution (Fig. 3*b*). The higher resolution values obtained for ΔN-p97–ADP, ΔN-p97-apo and p97-apo are likely overestimated because no features were lost when these maps were low-pass filtered to 24 Å resolution. Therefore, all volumes shown in this study were low-pass filtered to 24 Å resolution.
[3]The ΔN-p97-AMP-PNP volumes calculated from data recorded on films and on the CCD were identical.

isks, Fig. 4*d*). These observations suggest that the structural elements close to the center of the bottom ring are mobile.

At first glance, the side protrusions near the central plane of the p97 and ΔN-p97 structures look similar in shape to the "fin-shaped densities emanating from the upper ring" of VAT attributed to the N-domains[34]. However, because these side protrusions were observed in both ΔN-p97 and full-length p97 maps, they cannot be the N-domains of p97. Interestingly, no side protrusions have been observed near the central plane of VAT[32,34]. Notably, there are an extra ~50 amino acids at the C-terminus of p97 not present in VAT[44], suggesting that the side protrusions observed in our EM maps could be the C-terminal extensions of p97. Another possibility is that these side extensions are the linker between D1 and D2 or an as yet unknown structural element within the D2 domain. Taken together, the above observations support the following domain assignments in the 3D maps: the N-domains, seen only in the ADP-AlF_x state, are bound to the D1 hexamer (top ring), and D2 (bottom ring) is positioned slightly out of register below D1.

The 3D maps of full-length p97 and the deletion mutant ΔN-p97 are consistent with previous observations[30,32,34]. Our p97–ADP structure is similar to the previous published structure from Zhang and colleagues[30]. In particular, the top ring appears closed in both studies ('closed ring')[30], and the bottom ring ('open ring')[30] has a large central opening and six additional side protrusions. However, our assignment based on the ΔN-p97 data and the fit to the N-D1 crystal structure (PDB entry 1E32)[30] led us to the opposite assignment of the D1 and D2 domains. We have assigned the closed (top) ring as the D1 domains and the ring with the larger axial opening (bottom ring) as the D2 domains. The conserved handedness between the D1 and D2 rings and the similarity of sections taken from both rings is suggestive of a head-to-tail arrangement of the D1 and D2 domains. However, this proposed head-to-tail arrangement and the tail-to-tail arrangement proposed by Zhang and colleagues[30] both remain tentative[34] because of the lack of high-resolution information for the D2 domain.

Conclusion

The work presented here brings new insight into how p97 transforms the energy from ATP binding and hydrolysis into mechanical movements, some of which likely extend to other related proteins within the AAA family. Future biochemical and structural studies with co-factors and substrates should provide valuable information to understand which of the observed conformational changes impose forces on substrates directly or *via* such adaptors.

Methods

Sample preparation. Full-length p97 (residues 2–806, generous gift of G. Warren) and ΔN-p97 (residues 197–805, generous gift of S.W. Whiteheart) fused to an N-terminal His_6-tag were expressed in *Escherichia coli* M15 cells containing the pREP4 selection plasmid (Qiagen). The proteins were purified by successive passage over a Ni^{2+}-NTA agarose column (Qiagen) and a gel filtration column (Amersham Biosciences). The buffer used for the final elution contained 25 mM Tris, pH 7.5, 300 mM KCl, 5 mM β-mercaptoethanol, 1 mM EDTA, 10% (v/v) glycerol and 1 mM ATP for ΔN-p97, and 10 mM Tris, pH 8.9, 100 mM NaCl, 1 mM ADP–$MgCl_2$ or 1 mM ATP–$MgCl_2$ and 5 mM β-mercaptoethanol for p97. Fractions containing pure protein were pooled and concentrated using Millipore concentrators. Protein concentrations were estimated using the Bradford method.

The ATPase activity of the pooled protein fractions was determined by adding ATP in ~10-fold molar excess to the p97 hexamer

and measuring evolved P_i over a 2 h period at 22 °C with the Enzchek Phosphate Assay kit (Molecular Probes). The ATPase activity of p97 was ~12 μmol ATP mg^{-1} h^{-1}, in agreement with values published elsewhere[17].

For ΔN-p97, bound nucleotides were exchanged using a desalting column (Amersham Biosciences) equilibrated in 25 mM HEPES, pH 7.4, 400 mM KCl, 10% (v/v) glycerol and 5 mM β-mercaptoethanol or the same buffer containing either 2 mM AMP-PNP–$MgCl_2$ or 2 mM ADP–$MgCl_2$. For the full-length protein, the nucleotide exchange was performed identically except that the buffer contained 25 mM HEPES, pH 7.4, 100 mM KCl, 2 mM β-mercaptoethanol, 2 mM $MgCl_2$ and 2 mM AMP-PNP or ADP or no nucleotide. For the nucleotide-free states, the proteins were further incubated with apyrase (10 units ml^{-1}; Sigma) for at least 2 h on ice. For the ADP-AlF_x state, the protein in the ADP buffer was first diluted to 100 μg ml^{-1} and then incubated for ~6 h at 4 °C with 2 mM ADP, 8 mM NaF and 2 mM $AlCl_3$, in imidazole, pH 7. Proteins were diluted to 100 μg ml^{-1} in the above buffers and then applied to glow-discharged Quantifoil grids (Quantifoil Micro Tools GmbH), blotted and frozen in liquid ethane slush.

EM data acquisition. Frozen hydrated grids of p97 or ΔN-p97 were observed on a Philips CM200FEG microscope at 120 kV. Images were either recorded on films or on a Teitz 2K × 2K × 16 bit CCD camera (Table 1) under low dose conditions (~10 e^- $Å^{-2}$). Images recorded on films were taken at a nominal magnification of 50,000×. The quality of micrographs was assessed by optical diffraction, and micrographs were digitized on a Zeiss scanner with a 7 μm pixel size. Groups of 3 × 3 pixels were averaged, giving a pixel size of 21 μm on the micrographs or 4.1 Å on the specimen. Images recorded on the CCD were taken at a nominal magnification of 66,000×, with a pixel size of 3.7 Å. To facilitate the selection of particles, defocus pairs were taken so that the second image was 1 μm more defocused than the first. Only particles from the first image were included in the reconstruction.

Image analysis — starting model. For the ΔN-p97–AMP-PNP map, two starting models were initially used. The first model was a map of p97 obtained from negative stain and conical tilt method (I.R., unpub. data). The second model was a volume calculated from the PDB file of NSF D2 (PDB entry 1NSF)[29]. Two NSF D2 rings were staggered on top of each other and filtered to 50 Å resolution to obtain the 'rough' shape of the molecule. Two maps were calculated as described below using the two different starting models. Refinements were done using a starting angular increment of 15°, which was then reduced to 10° and 5°. The known six-fold symmetry of the complex[30,33] was imposed. Because no densities were lost by applying six-fold symmetry to the projection maps[33], the absence of defined densities in the 3D maps is unlikely a consequence of enforcing the symmetry but is most likely due to the flexibility of the corresponding domains. After refinement at 5° angular increment, the two maps converged to the same structure, suggesting that the starting models did not introduce a bias into the reconstruction. This volume was then used throughout as the starting model to calculate 3D EM maps of p97 and ΔN-p97 in all of the nucleotide conditions.

Image analysis — refinement procedure. Images were analyzed using the SPIDER package[45], and 3D maps were calculated following the projection matching methodology. The angular increments used were 15°, 10° and then 5° for p97 and ΔN-p97, followed by 2° and 1° for p97. For each angular increment, the raw data were aligned first with the projections of the model (the number of projections reflecting the six-fold symmetry). Because the orientation distribution of the particles varied between grids and to be able to compare several 3D maps, we were careful not to introduce artifacts resulting from overrepresentation of preferred views[46]. Therefore, we limited the number of particles included in the reconstruction to that of the smallest view-group. A new volume was calculated from the aligned images using the iterative back projection method. The new volume was used for a new round of alignment with reference matching. This step was repeated until <5% of the particles varied in orientation from half the initial refinement angles (15°, 10° and 5°) and <1% for the smaller angles. The total number of particles and the number of particles used per view are indicated in Table 1. After the final refinement, the particles were put into different defocus groups (Table 1, the defocus was determined from the full micrographs or CCD images) and intermediate volumes were calculated by the iterative back projection method and merged by Wiener filtering. The volumes obtained changed greatly during refinement with the 15°, 10° and 5° increment steps and little during refinement with the smaller increment steps. The handedness of the ΔN-p97 was determined by comparison with the D1 crystal structure (Fig. 4c). The handedness of p97 was determined so that it was the same as ΔN-p97. Thresholds used for the surface representation of the 3D maps were estimated using the constant of 0.866 Da $Å^{-3}$.The resolution was estimated by Fourier shell correlation using two 3D maps, each one calculated from half of the total data set and a cut-off value of 0.5.

Fitting of the EM data and the X-ray structures. Fitting of the D1 atomic structure in ΔN-p97–AMP-PNP was done with Situs[47]. Fitting the N and D1 atomic structures in the p97 maps was not as straightforward because these domains are in a different conformation and will require further investigation.

Acknowledgments

This work was supported by National Institutes of Health grants to R.A.M., E.M.W.-K. and W.I.W. A.P.M. was funded by a Wellcome Trust Prize International Traveling Fellowship. We thank P. Chacon for doing the fitting with Situs[47] and B. Sheehan for computing help. We also thank S. Kaiser, M. Bowen and C. Moores for critical reading of the manuscript.

Competing interests statement

The authors declare that they have no competing financial interests.

Received 8 July, 2002; 15 October, 2002.

1. Peters, J., Walsh, M.J. & Franke, W.W. An abundant and ubiquitous homo-oligomeric ring-shaped ATPase particle related to the putative vesicle fusion proteins Sec18p and NSF. *EMBO J.* **9**, 1757–1767 (1990).
2. Rabouille, C. *et al.* Syntaxin 5 is a common component of the NSF- and p97-mediated reassembly pathways of Golgi cisternae from mitotic Golgi fragments *in vitro*. *Cell* **92**, 603–610 (1998).
3. Roy, L. *et al*. Role of p97 and syntaxin-5 in the assembly of transitional endoplasmic reticulum. *Mol. Biol. Cell* **11**, 2529–2542 (2000).
4. Hetzer, M. *et al*. Distinct AAA-ATPase p97 complexes function in discrete steps of nuclear assembly. *Nature Cell Biol*. **3**, 1086–1091 (2001).
5. Shirogane, T. *et al*. Synergistic roles for Pim-1 and c-Myc in STAT3-mediated cell cycle progression and antiapoptosis. *Immunity* **11**, 709–719 (1999).
6. Madeo, F., Fröhlich, E. & Fröhlich, K. A yeast mutant showing diagnostic markers of early and late apoptosis. *J. Cell Biol*. **139**, 729–734 (1997).
7. Madeo, F., Schlauer, J., Zischka, H., Mecke, D. & Fröhlich, K. Tyrosine phosphorylation regulates cell cycle-dependent nuclear localization of cdc48p. *Mol. Biol. Cell* **9**, 131–141 (1998).
8. Yamada, T. *et al*. p97 ATPase, an ATPase involved in membrane fusion, interacts with DNA unwinding factor (DUF) that functions in DNA replication. *FEBS Lett.* **466**, 287–291 (2000).
9. Dai, R.M., Chen, E., Longo, D.L., Gorbea, C.M. & Li, C.H. Involvement of valosin-containing protein, an ATPase co-purified with IκBα and 26 S proteasome, in ubiquitin-proteasome-mediated degradation of IκBα. *J. Biol. Chem*. **273**, 3562–3573 (1998).
10. Meyer, H.H., Shorter, J.G., Seemann, J., Pappin, D. & Warren, G. A complex of mammalian ufd1 and npl4 links the AAA-ATPase, p97, to ubiquitin and nuclear transport pathways. *EMBO J*. **19**, 2181–2192 (2000).
11. Yen, C. *et al*. Involvement of the ubiquitin-proteasome pathway in the degradation of nontyrosine kinase-type cytokine receptors of IL-9, IL-2, and erythropoietin. *J. Immunol*. **165**, 6372–6380 (2000).
12. Dai, R.M. & Li, C.H. Valosin-containing protein is a multi-ubiquitin chain-targeting factor required in ubiquitin-proteasome degradation. *Nature Cell Biol*. **3**, 740–744 (2001).
13. Ye, Y., Meyer, H.H. & Rapoport, T.A. The AAA ATPase cdc48/p97 and its partners transport proteins from the ER into the cytosol. *Nature* **414**, 652–656 (2001).
14. Braun, S., Matuschewski, K., Rape, M., Thoms, S. & Jentsch, S. Role of the ubiquitin-selective CDC48$^{UFD1/NPL4}$ chaperone (segregase) in ERAD of OLE1 and other substrates. *EMBO J*. **21**, 615–621 (2002).
15. Jarosch, E. *et al*. Protein dislocation from the ER requires polyubiquitination and the AAA-ATPase Cdc48. *Nature Cell Biol*. **4**, 134–139 (2002).
16. Rabinovich, E., Kerem, A., Fröhlich, K.U., Diamant, N. & Bar-Nun, S. AAA-ATPase p97/cdc48p, a cytosolic chaperone required for endoplasmic reticulum-associated protein degradation. *Mol. Cell. Biol*. **22**, 626–634 (2002).
17. Kondo, H. *et al*. p47 is a cofactor for p97-mediated membrane fusion. *Nature* **388**, 75–78 (1997).
18. Meyer, H.H., Kondo, H. & Warren, G. The p47 co-factor regulates the ATPase activity of the membrane fusion protein, p97. *FEBS Lett*. **437**, 255–257 (1998).
19. Koegl, M.T. *et al*. A novel ubiquitination factor, E4, is involved in multiubiquitin chain assembly. *Cell* **96**, 635–644 (1999).
20. Ghislain, M., Dohmen, R.J., Lévy, F. & Varshavsky, A. Cdc48p interacts with Ufd3p, a WD repeat protein required for ubiquitin-mediated proteolysis in *Saccharomyces cerevisiae*. *EMBO J*. **15**, 4884–4899 (1996).
21. Maurizi, M.R. & Li, C.H. AAA proteins: in search of a common molecular basis. International Meeting on Cellular Functions of AAA Proteins. *EMBO Rep*. **2**, 980–985 (2001).
22. Patel, S. & Latterich, M. The AAA team: related ATPases with diverse functions. *Trends Cell. Biol*. **8**, 65–71 (1998).
23. Neuwald, A.F., Aravind, L., Spouge, J.L. & Koonin, E.V. AAA+: a class of chaperone-like ATPases associated with the assembly, operation, and disassembly of protein complexes. *Genome Res.* **9**, 27–43 (1999).
24. Ogura, T. & Wilkinson, A.J. AAA+ superfamily ATPases: common structure — diverse function. *Genes Cells* **6**, 575–597 (2001).
25. Vale, R.D. AAA proteins. Lords of the ring. *J. Cell Biol*. **10**, F13–19 (2000).
26. Babor, S.M. & Fass, D. Crystal structure of the Sec18p N-terminal domain. *Proc. Natl. Acad. Sci. USA* **96**, 14759–14764 (1999).
27. Coles, M. *et al*. The solution structure of VAT-N reveals a 'missing link' in the evolution of complex enzymes from a simple βαββ element. *Curr. Biol*. **9**, 1158–1168 (1999).
28. May, A.P., Misura, K.M.S., Whiteheart, S.W. & Weis, W.I. Crystal structure of the N-terminal domain of N-ethylmaleimide-sensitive fusion protein. *Nature Cell Biol.* **1**, 175–182 (1999).
29. Yu, R.C., Jahn, R., & Brunger, A.T. NSF N-terminal domain crystal structure: models of NSF function. *Mol. Cell* **4**, 97–107 (1999).
30. Zhang X., *et al*. Structure of the AAA ATPase p97. *Mol. Cell* **6**, 1473–1484 (2000).
31. Peters, J. *et al*. Ubiquitous soluble Mg^{2+}-ATPase complex. A structural study. *J. Mol. Biol.* **223**, 557–571 (1992).
32. Rockel, B. *et al*. Structure of VAT, a CDC48/p97 ATPase homologue from the archaeon *Thermoplasma acidophilum* as studied by electron tomography. *FEBS Lett.* **451**, 27–32 (1999).
33. Rouiller, I., Butel, V.M., Latterich, M., Milligan, R.A. & Wilson-Kubalek, E.M. A major conformational change in p97 AAA ATPase upon ATP binding. *Mol. Cell* **6**, 1485–1490 (2000).
34. Rockel, B., Jakana, J., Chiu, W. & Baumeister, W. Electron cryo-microscopy of VAT, the archaeal p97/CDC48 homologue from *Thermoplasma acidophilum*. *J. Mol. Biol*. **317**, 673–681 (2002).
35. Lenzen, C.U., Steinmann, D., Whiteheart, S.W. & Weis, W.I. Crystal structure of the hexamerizatioN-domain of *N*-ethylmaleimide-sensitive fusion protein. *Cell* **94**, 525–536 (1998).
36. Yu, R.C., Hanson, P.I., Jahn, R. & Brunger, A.T. Structure of the ATP-dependent oligomerizatioN-domain of *N*-ethylmaleimide sensitive factor complexed with ATP. *Nature Struct. Biol*. **5**, 803–811 (1998).
37. Wittinghofer, A. Signaling mechanistics: aluminum fluoride for molecule of the year. *Curr. Biol*. **7**, R682–685 (1997).
38. Putnam, C.D. *et al*. Structure and mechanism of the RuvB Holliday junction branch migration motor. *J. Mol. Biol*. **311**, 297–310 (2001).
39. Sousa, M.C. *et al.* Crystal and solution structures of an HslUV protease-chaperone complex. *Cell* **103**, 633–643 (2000).
40. Bochtler, M., Song, H.K., Hartmann, C., Ramachandran, R. & Huber, R. The quaternary arrangement of HslU and HslV in a cocrystal: a response to Wang, Yale. *J. Struct. Biol*. **135**, 281–293 (2001).
41. Wang, J. A corrected quaternary arrangement of the peptidase HslV and ATPase HslU in a cocrystal structure. *J. Struct. Biol*. **134**, 15–24 (2001).
42. Wang, J. *et al*. Nucleotide-dependent conformational changes in a protease-associated ATPase HslU. *Structure* **9**, 1107–1116 (2001).
43. Lamb, J.R., Fu, V., Wirtz, E. & Bangs, J.D. Functional analysis of the trypanosomal AAA protein *Tb*VCP with *trans*-dominant ATP hydrolysis mutants. *J. Biol. Chem*. **276**, 21512–21520 (2001).
44. Pamnani, V. *et al.* Cloning, sequencing and expression of VAT, a CDC48/p97 ATPase homologue from the archaeon *Thermoplasma acidophilum*. *FEBS Lett.* **404**, 263–268 (1997).
45. Frank, J. & Radermacher, M. SPIDER and WEB: processing and visualization of images in 3D EM and related fields. *J. Struct. Biol*. **116**, 190–199 (1996).
46. Sorzano, C.O.S. *et al.* The effect of overabundant projection directions on 3D reconstruction algorithms. *J. Struct. Biol*. **133**, 108–118 (2001).
47. Wriggers, W., Milligan, R.A. & McCammon, J.A. Situs: a package for docking crystal structures into low-resolution maps from electron microscopy. *J. Struct. Biol*. **125**, 185–195 (1999).
48. Jones, T.A., Zou, J-Y., Cowan, S.W. & Kjeldgaard, M. Improved methods for the building of protein models in electron density maps and the location of errors in these models. *Acta Crystallogr. A* **47**, 110–119 (1991).